Tissue Localization and Solubilities of αA-crystallin and its Numerous C-terminal Truncation Products in Pre- and Postcataractous ICR/f Rat Lenses

David R. Stella,[1,2] *Kyle A. Floyd,*[2,3] *Angus C. Grey,*[4,5] *Matthew B. Renfrow,*[1,6] *Kevin L. Schey,*[4] *and Stephen Barnes*[1,2,3,6]

Purpose. To investigate the tissue distribution and solubilities of various αA-crystallin truncation products in the cataractous ICR/f rat model.

Methods. Rat lenses from precataractous (21-day) and postcataractous (100-day) ICR/f rats were sectioned and applied to a matrix-assisted laser desorption/ionization-time-of-flight (MALDI-TOF) target plate. Mass spectrometry images were collected to obtain a macromolecular profile of the abundant lens proteins. Separately, age-matched lenses were extracted into water-soluble (WS) and water-insoluble/urea-soluble (WI-US) fractions and subjected to MALDI-TOF mass spectrometry to correlate the protein solubilities with the imaging data. Protein identities were assigned by using a top-down proteomics approach on a high-resolution mass spectrometer.

Results. Ten novel αA-crystallin truncation products were identified, along with six previously known αA-crystallin truncation products. Nearly all truncations exhibited nuclear localization, with larger truncated products displaying a ringlike localization that progressed outward toward the extranuclear, cortical region. The distributions were similar in both ages with the only significant difference being the amount of tissue area encompassed by a particular species with increasing age. Almost all nuclear products fractionated into the WI-US fraction, whereas the five largest extranuclear species exhibited mixed solubility.

Conclusions. A successful methodology for the sectioning and imaging of pre- and postcataractous ICR/f rat lenses has been established. Data collected from these analyses indicate that there are multiple αA-crystallin truncation products present in both pre- and postcataractous rats. Furthermore, these species have defined lenticular localizations and unique solubilities that may be a consequence of lens development and protein function within the lens environment. (*Invest Ophthalmol Vis Sci.* 2010;51:5153–5161) DOI:10.1167/iovs.10-5302

The ocular lens is an intriguing tissue, in part because of its atypical development and differentiation. The lens is formed by primary fiber cells derived from the ectoderm during early embryonic development that eventually become the lenticular nucleus.[1] Subsequently, mature fiber cells (derived from a monolayer of epithelial cells present on the anterior surface of the lens) elongate to wrap around this nucleus, forming concentric layers.[1] As a requirement for light transmission, the mature fiber cell is programmed to degrade all cellular organelles, rendering it incapable of further protein synthesis.[2] Because of this, the lens retains all proteins that were synthesized before terminal fiber cell differentiation. This phenomenon is remarkable, as the lens must maintain transparency to function while possessing very high protein concentrations (greater than 320 mg/mL in humans[1]), which are necessary to refract and focus incoming light.

The crystallins are the most abundant class of proteins in the human lens[3] and are subdivided into three major groups, the α-, β-, and γ-crystallins, each having a particular function. The α-crystallins, comprising nearly half of the total soluble lens proteome,[4] are ~20-kDa proteins that form large molecular mass aggregates ranging upward from 800 kDa when complexed with substrates.[4,5] They are small heat shock proteins possessing a chaperone-like function for binding and sequestration of denatured protein substrates.[4,6] There are two subtypes of the α-crystallins, the αA and αB, with ~60% sequence homology, that can form hetero-oligomers within the lens environment at a 3:1 ratio.[1,7] These large complexes help to maintain the solubility of denatured lens proteins to prevent aggregation, a hallmark of cataract formation.

We studied cataract progression by using a whole-tissue approach involving matrix-assisted laser desorption/ionization-time-of-flight (MALDI-TOF) mass spectrometry imaging (MSI). This technique permits the detection and analysis of ionizable macromolecules within a tissue section by mass spectrometry, while retaining tissue distribution and localization.[8] It is similar to classic immunohistochemistry, but is enhanced because MALDI-TOF MSI is not limited by antibody availability or specificity and simultaneously produces a chemical pro-

From the Departments of [1]Biochemistry and Molecular Genetics and [3]Pharmacology and Toxicology, the [6]Biomedical FT-ICR Laboratory, and the [2]Purdue University-University of Alabama at Birmingham Botanicals Center for Age-Related Disease, University of Alabama at Birmingham, Birmingham, Alabama; and the [4]Department of Biochemistry, Mass Spectrometry Research Center, Vanderbilt University, Nashville, Tennessee.

[5]Present affiliation: Department of Optometry and Vision Science, University of Auckland, Auckland, New Zealand.

Supported by Grant FY2007-08-84 from the EyeSight Foundation of Alabama; P50 AT00477 from The National Center for Complementary and Alternative Medicine and the NIH Office of Dietary Supplements to the Purdue University-University of Alabama (UAB) at Birmingham Botanicals Center for Age-related Disease (Connie M. Weaver, PI); and EY13462 from the National Institutes of Health (NIH) (KLS). Funding for the purchase of the mass spectrometers at the University of Alabama at Birmingham came from NIH/NCRR (National Center for Research Resources) Shared Instrumentation Grants S10 RR13975-01 and RR17261-01 (SB). Funds for the operation of the UAB Biomedical FT-ICR MS Laboratory were provided in part by the supporters of the UAB Comprehensive Cancer Center and the Department of Biochemistry and Molecular Genetics.

Submitted for publication February 1, 2010; revised April 1, 2010; accepted April 6, 2010.

Disclosure: **D.R. Stella**, None; **K.A. Floyd**, None; **A.C. Grey**, None; **M.B. Renfrow**, None; **K.L. Schey**, None; **S. Barnes**, None

Corresponding author: Stephen Barnes, Department of Pharmacology and Toxicology, McCallum Research Building, Room 452, University of Alabama at Birmingham, 1918 University Boulevard, Birmingham, AL 35294; sbarnes@uab.edu.

file of tens to hundreds of ionizable protein species present across the tissue section during a single experiment.[9] MALDI-TOF MSI typically allows for the detection of ionizable proteins within the range of 1,000 to 50,000 Da,[10] which is amenable to lens tissue studies because of the small average monomeric protein molecular masses of the abundant crystallin proteins (~20 kDa).[1]

In the present study, we used tissue sections from both pre- (21 days of age) and post-cataractous (100 days of age) ICR/f rat lenses (Fig. 1). This animal model of age-related cataract disease is derived from the Wistar rat.[11] Cataracts form in the ICR/f rat by ~10 weeks of age, with development beginning in the cortical region of the lens. As development continues, the opacification extends into the nuclear region, eventually producing a fully opaque lens cataract.[12] Although the exact cause is not fully understood, the development of the cataract in the ICR/f rat may result from an early oxidative insult derived from abnormalities in lipid metabolism.[13] As a result, changes within the lens microenvironment[14–17] are semipermanent, as the lens is incapable of synthesizing or degrading proteins. This early insult renders these animals susceptible to cataract formation as time progresses and the repair–maintenance mechanisms are depleted.

To our knowledge, this study is the first to use MSI to investigate a small rodent lens, as well as the first comparison of MSI data from pre- and postcataractous lenses obtained from a laboratory model of cataracts. By combining the MSI imaging data with subsequent MALDI-TOF MS analysis of water-soluble (WS) and water-insoluble/urea-soluble (WI-US) ICR/f lens protein extracts, we have observed specific properties at pre- and postcataract lens stages. In the ICR/f rat lens, the αA-crystallin protein and its numerous truncation products are segregated by spatial distribution (nuclear versus extranuclear) and their intrinsic solubilities. These truncations may not be the primary cause of the cataract, as these features were detected in both the early and late stages of development in the ICR/f lens.

Materials and Methods

All reagents used in the study were of the highest quality available. High-performance liquid chromatography (HPLC)–grade solvents, including acetonitrile (ACN), ethanol (EtOH), and methanol (MeOH), as well as pure formic acid (99%; FA), were purchased from Fisher Scientific (Pittsburgh, PA). Sinapinic acid (SA) was purchased from Sigma-Aldrich (St. Louis, MO), and the water was purified (Milli-Q purification system; Millipore, Billerica, MA). All animal procedures were performed with the approval of and within the guidelines set forth by the University of Alabama at Birmingham Institutional Animal Care and Use Committee and adhered to the ARVO Statement for the Use of Animals in Ophthalmic and Vision Research.

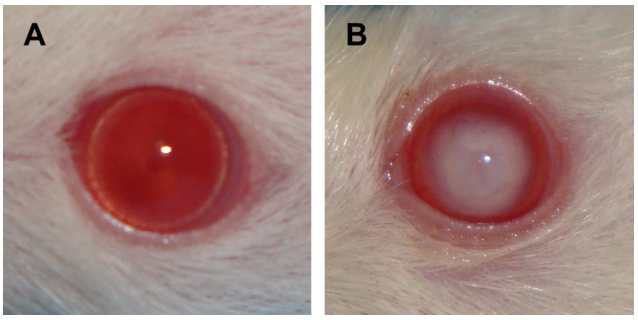

Figure 1. Photographs of ICR/f rat eyes show a clear lens at (**A**) 21 days and (**B**) a lens cataract at 100 days of age.

Tissue Sectioning and Processing

Frozen intact rat eyes (−80°C) were thawed, and lenses were dissected with the aid of a dissecting microscope (EZ4-D; Leica, Bannockburn, IL). The lenses were carefully extracted by corneal incision around the periphery of the eye. Care was taken to ensure the proper orientation of the lens, with the anterior side facing upward. The lenses were washed with deionized water to remove any contaminants and refrozen in a cryostat (CM3050-S; Leica, Bannockburn, IL) at −20°C, before sectioning. They were attached to the center of the cryostat chuck by layering optimal cutting temperature (OCT) medium. The lenses were sectioned into 20-μm slices, and thaw-mounted onto a methanol-layered, gold-coated MALDI plate (Applied Biosystems, Foster City, CA). Multiple sections were applied to each MALDI plate. After being placed on the plate, the sections were allowed to air-dry and then were washed with sequential submersion in 70% EtOH and 95% EtOH for 60 seconds per solution to remove lipids and salts and fix the proteins. The processed plates were then placed in a vacuum desiccator for at least 15 minutes before matrix deposition.

Matrix Deposition

Matrix was applied with an acoustic reagent multispotter device (Portrait 630 Spotter; Labcyte, Sunnyvale, CA) that is capable of delivering 170 pL of matrix solution per spot. The matrix (15 mg/mL SA in 50:40:10 ACN:H_2O:FA solution) was applied with a 400-μm offset-interleaving technique to achieve a final center-to-center spot distance of 200 μm across the entire tissue section. The spotter was operated in "fly-by" mode, which enables reapplication of the matrix at each spot for a total of 40 cycles (1 droplet/cycle), to ensure matrix saturation on the tissue.

MSI Analysis

Mass spectrometric analyses were performed in the linear, positive mode at a 20-kV accelerating potential on a time-of-flight mass spectrometer (Autoflex II Linear; Bruker Daltonik, Bremen, Germany) equipped with a laser (Smartbeam; Bruker Daltonik) capable of operating at a repetition rate of 200 Hz. The laser beam size was set to medium, estimated to be approximately 150 μm in diameter, at a laser power of 72%. A linear, external calibration was applied to the instrument before data collection, with a protein mixture of insulin ($M+H^+$ = 5,734), cytochrome C ($M+H^+$ = 12,361), myoglobin ($M+H^+$ = 16,952), and trypsinogen ($M+H^+$ = 23,982). Mass spectral data sets were acquired over lens sections with a raster step size of 200 μm obtaining 200 laser shots per spectrum (flexImaging software; Bruker Daltonik). After data acquisition, molecular images were reconstituted by the software. The data were smoothed with a Gaussian filter (width 2 *m/z*, four cycles), and baseline subtraction was applied by using the TopHat algorithm and normalized to total ion current with the software. Extracted peaks were plotted ±0.05% mass-to-charge units, to generate an image.

Lens Homogenization

ICR/f rat eye samples were obtained at 21 and 100 days of age. The lenses were dissected from frozen intact eyes and washed with deionized water. To collect the WS proteins, the lenses were homogenized with 50 mM Tris-HCl buffer (pH 7.4) containing protease inhibitors (Complete Protease Inhibitor Cocktail; Roche, Basel, Switzerland) using a Teflon homogenizer in a 1.5 mL microcentrifuge tube. The samples were centrifuged at 18,000*g* at 4°C for 15 minutes, and the supernatant saved. This step was repeated to remove as much of the WS proteins as possible. Finally, the pellets were homogenized in a similar Tris-HCl buffer supplemented with 6 M urea, to obtain the WI-US proteins.

MALDI-TOF Analysis of Extracts

Samples were quantified by using a BCA protein assay kit (Pierce Biotechnology, Rockford, IL), and read on a plate reader at 590 nm, to

obtain the concentration. Protein (12 μg) from each sample was washed and concentrated with a C_4-column (ZipTip; Millipore) eluted with 10 μL of 60% ACN and 0.1% TFA and dried in a centrifuge (SpeedVac; Agilent, San Diego, CA). Each sample was resuspended into 5 μL 50% ACN and 10% FA. An aliquot (1 μL) of the sample solution was mixed 1:1 with 15 mg/mL SA in 50% ACN and 10% FA and spotted onto a MALDI target plate (Bruker Daltonik). Spectra from these samples were collected on the same instrument as the tissue samples collecting data at a repetition rate of 100 Hz for a total of 2000 shots. The data were smoothed and baseline subtracted.

HPLC Fractionation of Lens Homogenates and FT-ICR Top-Down Proteomic Analysis

Protein separations were performed with an HPLC system (1100 Series; Agilent Technologies). ICR/f lens homogenates were loaded onto a 5-μm C5 column (250 × 2.0 mm ID; Jupiter 300; Phenomenex, Torrance, CA) pre-equilibrated with 5% ACN and 0.1% FA (buffer A) at a flow rate of 150 μL/min. Lens homogenates were eluted with a linear gradient of 2% to 50% buffer B (95% ACN/ 0.1% FA) over 40 minutes. The column eluate was collected with an automated fraction collector (Agilent Technologies) at 1-minute intervals into sterile 96-well plates (Eppendorf twin.tec, Hauppauge, NY). After each separation, the samples were dried in a centrifuge (SpeedVac; Agilent). The samples were resuspended in 30 μL of 50% ACN and 0.1% FA.

Individual fractions were directly injected into a 7-T mass spectrometer (LTQ FT-ICR; Thermo Scientific, Waltham, MA) via a chip-based infusion system (TriVersa NanoMate; Advion, Ithaca, NY). With each sample, a new spray nozzle was used to limit cross-contamination. High-resolution mass scans (*m/z* 200–2000) were performed in the FT-ICR cell with a resolution of 200,000 at *m/z* 400. Full scans were processed to deconvolute >2+ charge states to $M+H^+$ (Xtract software package within the Xcalibur software; Thermo Scientific), with the setting of S/N, 2; fit factor, 44%; remainder, 25%; averaging table and a maximum charge state, 30. Individual charge states were manually isolated in the LTQ and fragmented by using CID (collision-induced dissociation) with N_2 gas at 20% maximum intensity. Fragmentation spectra were collected as FT-ICR scans and analyzed (Xtract software; Thermo Scientific). De-isotoped MH^+ precursor ions and fragment ions were submitted to an online engine (MS-Tag; http://prospector.ucsf.edu/prospector/html/instruct/tagman.htm/ provided in the public domain by the University of California San Francisco) and searched against the UniProt *Rattus norvegicus* database to obtain protein identities from the MS/MS spectra (www.uniprot.org/ The UniProt Consortium).[18]

Results

MSI Analysis of Pre- and Postcataractous ICR/f Rat Lens Sections

Figure 1A shows a precataractous (21-day old), visibly transparent ICR/f rat lens, and Figure 1B shows a cataractous (100-day old) ICR/f rat lens in which there is a dense opacification throughout the entirety of the lens. Lenses such as these were used to evaluate changes in protein distribution and solubility during cataract development. Figure 2 shows the sectioned lens tissues and selected *m/z* signals that were obtained from 21-day (Figs. 2A–D) and 100-day (Figs. 2E–H) ICR/f rat lenses. In the optical images (Figs. 2A, 2E), there are obvious regions that are segmented by slight color changes (from white to translucent against the gold background of the MALDI target plate) that appear at various radii from the center of the tissue. These regions represent different stages of lens development, as the nuclear center was developed during embryogenesis with subsequent addition of lens fiber cells.[19] From this, it is plausible to predict regional differences in protein signals, as these regions were formed at different points during lens development. We confirmed this by extracting images from the MSI experiment as indicated in Figures 2B–D and 2F–H. For this purpose and for reasons discussed later, two of the major protein species present in the MSI experiment were chosen for analysis. The first protein is the N-terminally acetylated, full-length αA-crystallin (residues 1-173) protein, at an average mass of 19,835 Da ± 0.06% (Figs. 2B, 2D, 2F, 2H,

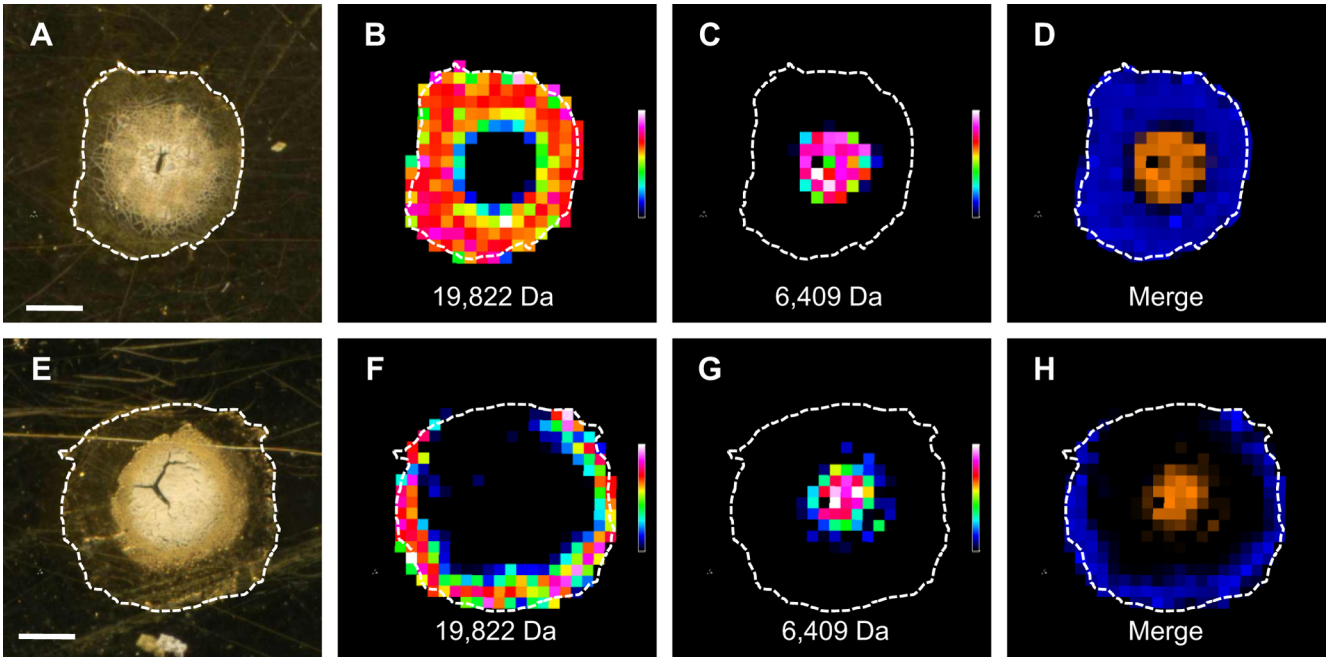

Figure 2. MALDI-TOF MS images of ICR/f rat lens sections: (**A–D**) 21-days of age and (**E–H**) 100-days of age. (**A**, **E**) Optical image of lens sections against a gold MALDI target plate. (**B**, **F**) Heat-map image with areas of high abundance shaded in *white* and *red* and areas of low abundance shaded in *blue* and *black*, of the 19,822 Da ion. (**C**, **G**) Heat-map image of the 6,409 Da ion. (**D**, **H**) Merged image of both 19,822 Da (*blue*) and 6,409 Da (*orange*) ion signals. Scale bar, 1 mm, with all images on the same scale.

blue). The second protein is an N-terminally acetylated αA-crystallin truncation product (residues 1-53), at an average mass of 6413 Da ± 0.11% (Fig. 2C, 2D, 2G, 2H, orange). Although other MSI studies have localized low-molecular-weight αA-crystallin truncation products (1-40, 1-50, and 1-58) to the nuclear core of other species,[20–22] this is study is the first to identify the 1-53 truncation product as a major protein present in the lens.

The distribution of the full-length αA-crystallin in these rat lenses is in agreement with previous lens MSI studies, where it was found to associate only in the outermost cortical regions, whereas other posttranslationally modified forms (phosphorylated and truncated) were found to localize to subcortical regions deeper within the lens tissue.[20–22] Despite the full-length αA-crystallin being present in lenses of both ages, the key distinguishing factor is the approximate 30% reduction in its cross-sectional area in the 100-day ICR/f lens (compare Fig. 2B with 2F). Grey et al.[22] recently showed a reduction in the full-length αA-crystallin abundance in progressively aged human lenses. In the rat lens, the αA-crystallin truncation product specifically localizes to the nuclear region, encompassing the whitest regions present in the optical tissue sections (Figs. 2C, 2G). Surprisingly, there appears to be no difference in the cross-sectional area of this product between the two different lenses, given their different ages and stages of cataract development.

The MSI data indicate three broad classes of radial protein distributions, which are depicted in Figure 3. Nuclear distribution was defined by the boundaries of the 1-53 αA-crystallin truncation product present in all lenses analyzed (dashed lines). The second boundary is defined as the nuclear ring that displays a ring-like distribution immediately outside the nuclear region that grows with age. The final class of lens protein distributions identified is the cortical distribution, in which the proteins fall beyond the nuclear ring and also display a ringlike presence, with the outermost region being defined by actively growing–dividing epithelial cells. As previously mentioned, these different distributions may represent different regions of the lens throughout the periodic stages of development. The complete MSI data are presented in Figure 4. Here, all the discernible peaks correlating to the αA-crystallin and its truncation products are shown (the protein identities are discussed later). Most of the distribution profiles are preserved between the different-aged sections with the most obvious difference being both the diffusion of particular species in the 100-day section (bottom) versus the 21-day section (top) and the reduced cross-sectional area of both full-length αA-crystallin species (the normal protein and the A-chain).

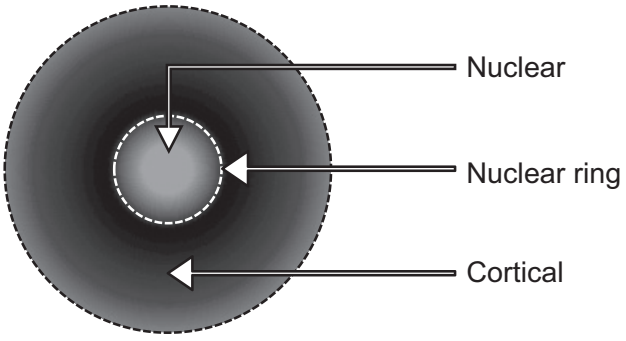

FIGURE 3. Regional protein and peptide distributions identified by MALDI-TOF MSI of the ICR/f rat lens.

Solubility Analysis of Cataractous ICR/f Rat Lens Proteins

Although Figures 2D and 2H indicate a clear partition of the αA-crystallin and its truncation product within the tissue, they provide no information about their solubility characteristics. This parameter is very important, because it is the basis on which the development and progression of the age-related cataract is posited. By fractionating whole lens homogenates into WS and WI-US fractions and using standard MALDI-TOF MS analysis, we were able to correlate the MSI signals with their intrinsic solubilities. As indicated in Figure 5A, the full-length αA-crystallin was found to be highly enriched within the WS lens fraction in both 21-day (dashed black line) and 100-day (dashed gray line) lens protein extracts, although the corresponding WI-US proteins (solid black and solid gray lines) have minimal intensities. This information indicates that the full-length αA-crystallin is freely soluble when present in both the pre- and postcataractous lens tissue. Given the functions of the full-length αA-crystallin, these data were not surprising. However, the observed WI-US distribution of the 1-53 amino acid residue truncation of the αA-crystallin (Fig. 5B) was of great interest. Combining this discovery with its tissue distribution, it becomes apparent that the nuclear regions of both lenses contain protein/peptide species that are present in a WI state well before the development of a visible nuclear cataract.

In the 21-day ICR/f lens, the tissue was transparent (Fig. 1A) and contained limited light-refracting precipitates, although its 100-day counterpart (Fig. 1B) was fully opaque. The MSI and solubility data alone did not reveal a significant difference between the two lenses. By observing the mass spectral profiles of the two ages (Fig. 6), one can see a level of uniformity between the ages in the WS and the WI-US profiles. Figure 6A shows the WS profile comparison of the 21-day (dashed black line) and the 100-day (dashed gray line) ICR/f rat lens extracts. With few exceptions, nearly all the signals that were present in the 21-day lens were also present in the 100-day lens, indicating that the most abundant WS signals did not correlate directly with the development of the cataract. For the most abundant WI-US samples (Fig. 6B), there were peaks that were common to both, but new species (asterisks) began to appear in the 100-day ICR/f rat lens (solid gray line). These signals may correspond to various truncation products, such as the 1-53 αA-crystallin C-terminal truncation discussed earlier, that result from proteolytic events occurring in the ICR/f rat lens.[15,17] Although these data show an increase in WI-US truncation products over time, again, they demonstrate that some protein species do not directly correlate with cataract development, as they were present in the pre- as well as postcataractous lenses.

Identification of Protein Signals in the MSI and Solubility Datasets

Having identified multiple peaks by MSI that are fractionated by tissue localization and/or discrete solubility characteristics, it was then necessary to determine each peak's identity. MSI is a useful tool in providing information on the distribution and localization of the most abundant ionizable protein species within a tissue section; however, it lacks the capability of providing the exact identity of those peaks. The observed species were identified by analyzing the *m/z* signals detected in the previous MALDI-TOF experiments (both the MSI and solubility profiling) with a top-down directed mass spectrometry approach, as outlined in Figure 7. By analyzing the accurate mass of the abundant protein species on a hybrid linear quadrupole ion trap (LTQ) 7-T Fourier transform-ion cyclotron resonance mass spectrometer (FT-ICR MS), identification could be made in silico, based on mass matching of the N-terminally acetylated αA-crystallin protein and its possible truncation

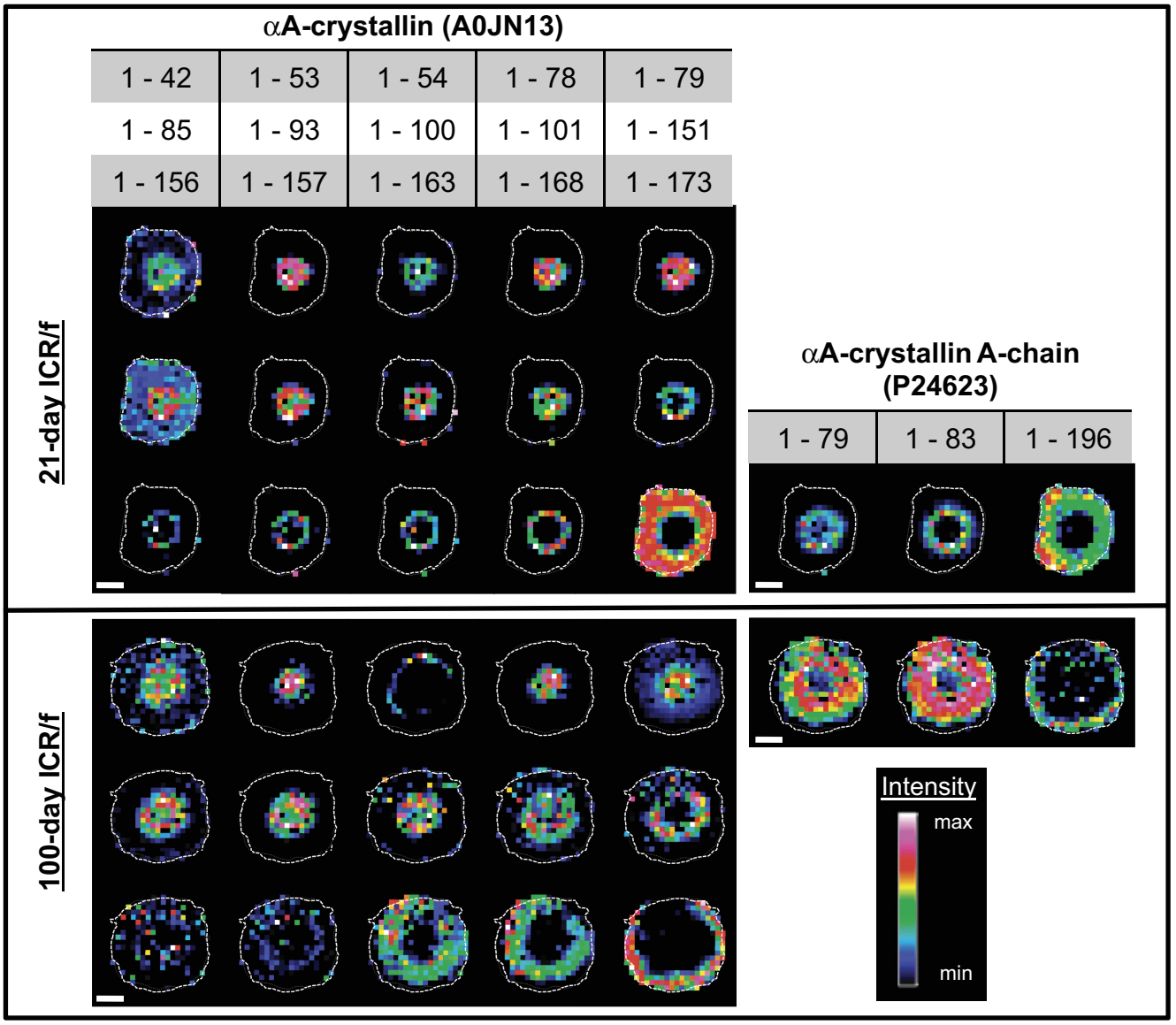

FIGURE 4. Complete MALDI-TOF MSI data set for both the 21-day (*top*) and 100-day (*bottom*) ICR/f rat. The heat map indicates the abundance of the particular αA-crystallin species, as indicated at the *top* of the figure. Scale bar, 1 mm, with all images on the same scale.

products (Figs. 7A, 7B). When the FT-ICR mass spectrometer detects a multiply charged ion (the $[M+5H]^{5+}$ molecular ion), a deconvoluted, accurate monoisotopic mass can be assigned (Fig. 7B, 6409.26 Da). Comparatively, the peak that corresponds to this value in the MSI data was within 0.11% of this mass, indicating a very close association of these peaks based on both the mass and the abundance. The mass accuracy of the FT-ICR data alone are sufficient to identify this peak as the

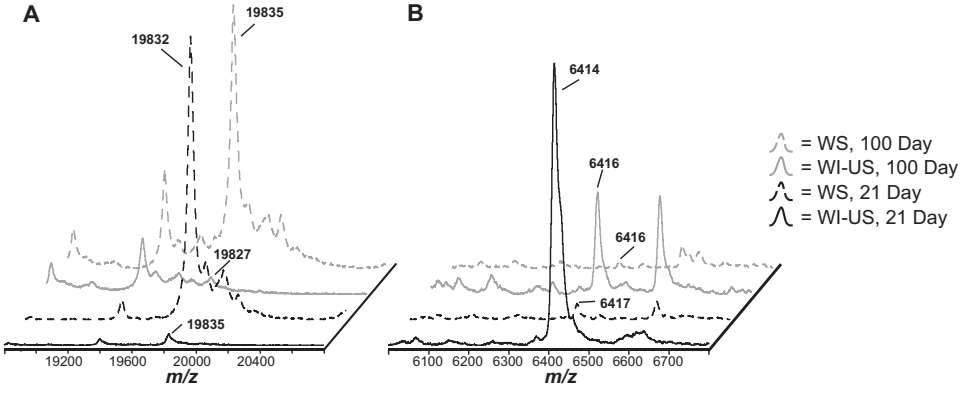

FIGURE 5. MALDI-TOF spectra highlighting the water-solubility profiles of (**A**) the full-length αA-crystallin, 19,835 Da ± 0.06%, and (**B**) the αA-crystallin truncation product (1-53 aa residues), 6,413 Da ± 0.11%. *Solid lines* WI-US fractions; *dashed lines*: WS samples.

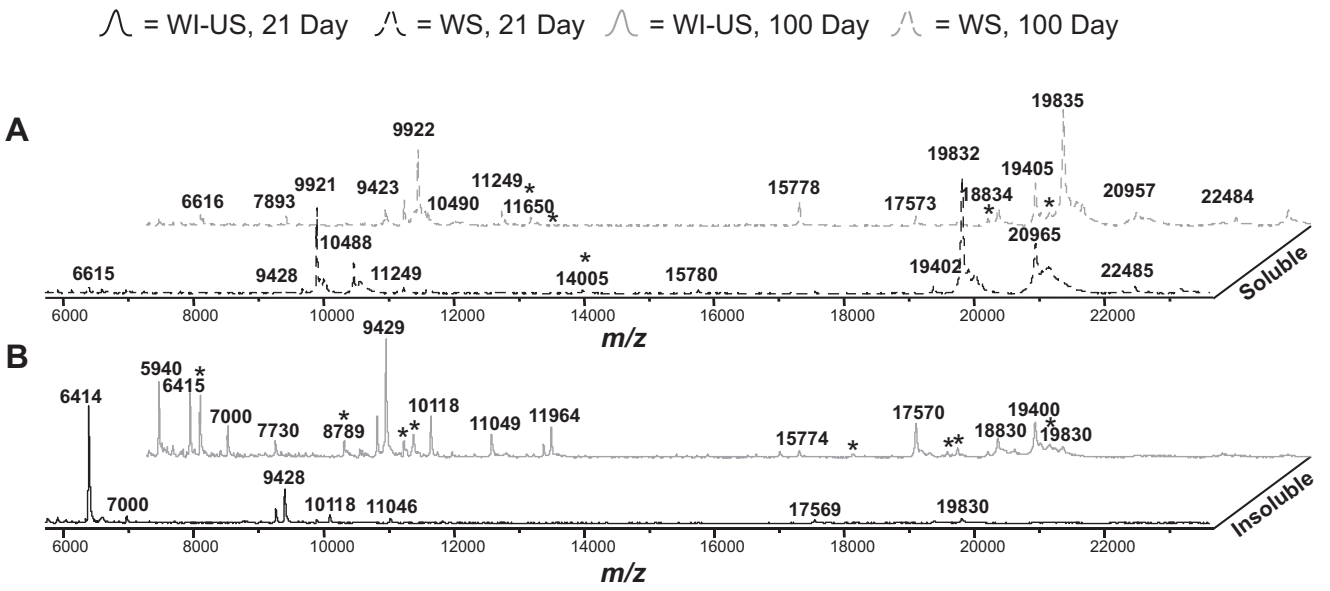

FIGURE 6. Broad-range (6,000–23,000 Da) MALDI-TOF spectra showing the water-solubility characteristics of the (**A**) WS and (**B**) WI-US fraction. WI-US fractions are indicated by *solid lines*; WS fractions are indicated by *dashed lines*: 21-day ICR/f (*black*) and 100-day (*gray*) ICR/f rat lens homogenate. *Novel peaks detected between the compared spectra.

N-terminally acetylated αA-crystallin truncation product (residues 1-53), based on the calculated mass of 6409.19 Da (~14 ppm mass accuracy). However, top-down proteomics provides a partial amino acid sequence tag to confirm a protein assignment. In this case, a specific *m/z* value (precursor ion series, Fig. 7A) can be isolated in the ion trap and subjected to CID via inert nitrogen gas yielding fragment ions. These fragment ions, which are indicative of sequential cleavage of amino acid residues, are then transferred into the FT-ICR MS for *m/z* detection (Fig. 7C). This permitted accurate mass analysis of the fragment ions for submission to an online MS-Tag search engine to validate the previously associated protein identification.

With this approach, 18 different species of the αA-crystallin were identified (Table 1). Of these 18 species, only 6 have been identified in the ICR/f rat,[17] another was found in a similar MSI study[22] (residues 1-101), two were variations of the full-length αA-crystallin, and the remaining nine were novel truncation products. Most of these products were C-terminally truncated forms exhibiting specific tissue localization and solubility characteristics as summarized in Table 1. In general, the smaller the truncation product, the more likely that it was localized toward the nuclear region of the lens as well as a tendency to be WI-US. All these identified αA-crystallin truncation products were found in both ages, regardless of cataract status. The most notable difference was a dispersion and expansion of all truncation products larger than 151 residues with age. Each of these species exhibited a nuclear ring organization at the precataractous stage, only to become more diffuse and larger in surface area at the postcataractous stage. Also observed was the limited distribution of the full-length αA-crystallin protein to the outermost regions in the postcataractous sections.

DISCUSSION

Cataract is often produced by a dysregulation of the folding of proteins in the lens that condense to form large, light-scattering precipitates. This may seem to be a simplistic view of cataract development, but the fact that lens proteins remain in place and contribute to transparency throughout the life of an organism adds a new level of complication. The ability of these proteins to survive in a dynamic environment with stressors that include oxidation,[23] deamidation,[24] and truncations,[25] as well as various chemical adducts with glutathione,[26] sugars, and other proteins/peptides,[23,27] while maintaining solubility is a significant departure from normal biochemistry. In this MALDI-TOF imaging study, αA-crystallin, the predominant lens crystallin, was distributed in different regions of the lens tissue according to its level of truncation. As a general rule, truncation products involving more than 10 C-terminal residues were found to colocalize near/within the nuclear region, the region that was formed during embryogenesis. Studies on αA-crystallin have shown that in aged lenses, multiple C-terminal truncations are present and that these products are altered in their chaperone capacities,[28] solubilities,[29] and the rate of subunit exchange within the complexes.[30] These altered capacities may dictate their co-localization to specific regions in the lens. If that notion is true, the various functions of the αA-crystallin would be associated with its localization and the particular functional requirements necessary for that region. Overall, such compartmentalization may help to establish the necessary chaperone functions, indices of refraction, and overall lens health.

Our MSI data indicate that specific proteins co-localize in the nucleus of the lens. In 1998, Sweeney and Truscott[31] described a nuclear barrier in aged human lenses that isolated the nucleus. This barrier is a product of lens development that occurs with age, and its formation may be the result of various biochemical events including the compaction of fiber cells,[32] membranes decorated with denatured proteins,[33] changes in membrane lipid composition,[33,34] and truncations occurring on the aquaporin water channels.[35] Studies have shown that water and glutathione, a major lens antioxidant, are reduced in their ability to diffuse into the nucleus which may prevent the delivery of nutrients and antioxidants to the nuclear core,[31,36] resulting in an altered proteomic profile that is specific to this region. Although the initial development of this nuclear barrier was studied in human lenses, lenses taken from Wistar rats (the ICR/f's parental strain) have shown that the nuclear core has similar exclusion properties. In two studies,[37,38] the MP20 protein, an abundant lens membrane protein, was found to

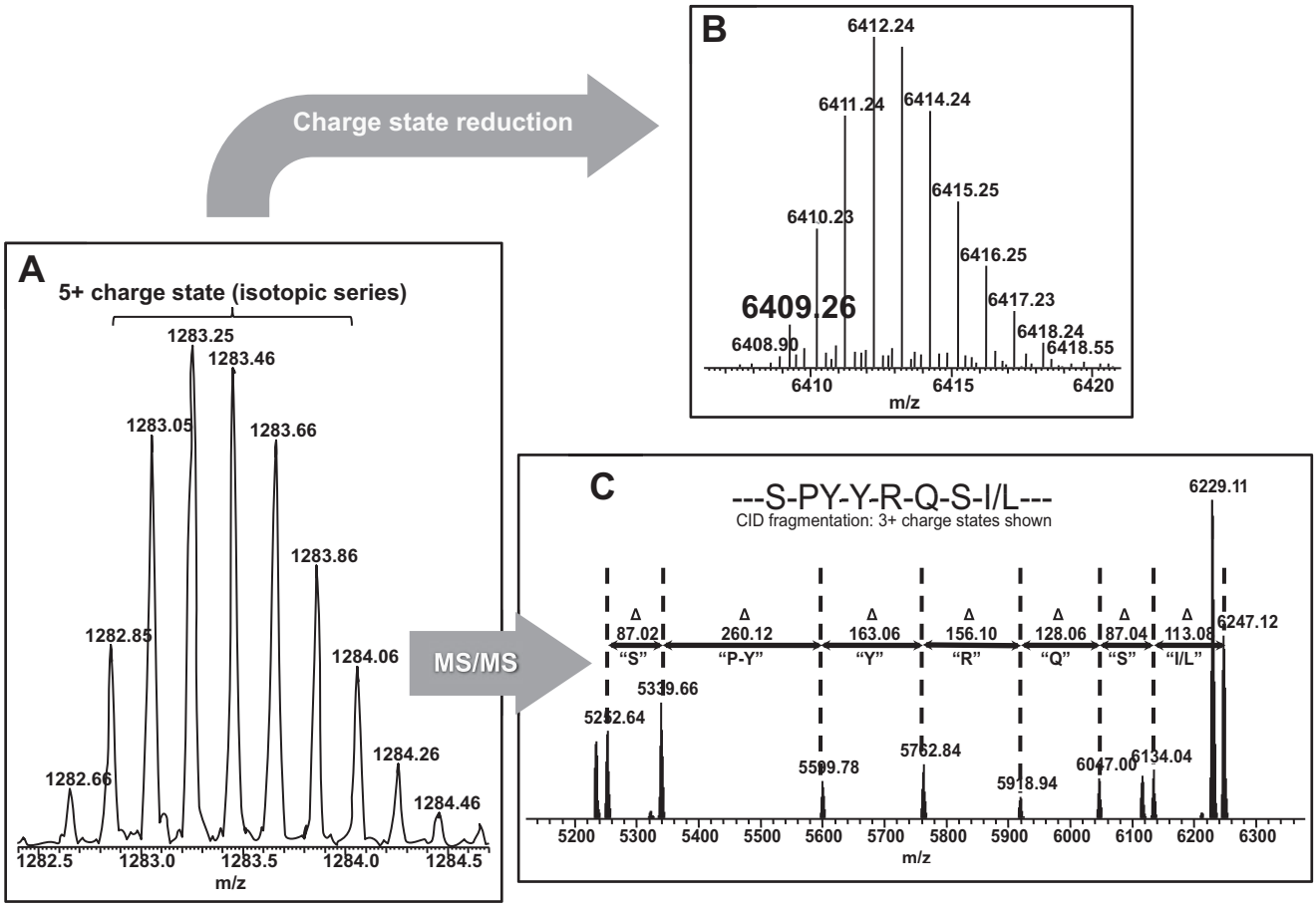

FIGURE 7. Workflow for top-down–directed protein identification on a 7-T LTQ FT-ICR mass spectrometer. (**A**) Initially, an isotopic distribution of a single charge state (here, $[M+5H^+]^{5+}$) for a given protein species is measured in the ICR cell of the mass spectrometer, to obtain a high-resolution spectrum. (**B**) This spectrum is then computationally deconvoluted into its $[M+H^+]^{1+}$ isotopic distribution, to determine its true mass (here, 6409.26 Da) for database comparison. (**C**) The $[M+5H]^{5+}$ ion is subjected to collision-induced dissociation in the ion trap (LTQ), causing fragmentation through collision with an inert gas where the excess kinetic energy of the ion is converted into peptide-bond breaking potential energy resulting in fragment ions to be measured in the high-resolution ICR cell. These data give a partial sequence of the selected precursor ion for database comparison.

redistribute from the cytoplasm to the cellular membrane in maturing fiber cells, by an unknown mechanism. This action was hypothesized to be the necessary impediment to dye accumulation in the nuclear core of the lens by a physical barrier.[38] In support of this, our study indicated αA-crystallin truncation products in the lenses of the ICR/f rat (as noted in Fig. 4) were also found to tightly surround the nucleus and thus may be involved in the development, function, and impermeable nature of this barrier.

Investigating the solubility of lens proteins by the use of mass spectrometry (Figs. 5, 6) showed the signals that were common between the cataractous states in both the WS and WI-US fractions. Associating the solubilities of the full-length and truncated αA-crystallin with the MSI data showed a trend for these products to be distributed in different regions of the lens on the basis of their solubility. The WI-US truncation products were found in the nuclear region, whereas the WS full-length αA-crystallin was exclusively in the extranuclear regions. The function of these truncation products and their localization to the nuclear core encourages the development of future hypotheses relating to the function of the N terminus of the αA-crystallin and its relation to multimerization and subunit exchange in its chaperone activities.[39,40] As previously stated, the preeminent difference between the sections was the amount of surface area covered by a particular species. The general trend was an increasing amount of αA-truncation products in the 100-day old ICR/f lens section. This process may be a result of fiber cell alterations and subsequent liquefaction that occurs as a result of cataract development in this laboratory animal model.[41] Another observation was the age-related, limited distribution of the full-length αA-crystallin proteins to the outermost periphery of the lens section. This distribution difference may be the result of fiber cell degeneration,[41] whereby the cellular contents of cortical fibers, including the αA-crystallin, are no longer contained within a single fiber cell. They are free to interact with other proteins (either folded or unfolded) within the lens cortex, to form cataractous aggregates that remain undetectable by the technology used in the present study.

That WI-US proteins are already present in the nuclear region of young precataractous ICR/f lenses demonstrates the importance of obtaining a more comprehensive understanding of the development of the cataract. The data in this study indicate that WI-US proteins may be a result of normal lens biology in this animal model and not necessarily the direct cause of cataract development. Although it is necessary to evaluate the αA-crystallin truncations discussed herein in the Wistar rat, it is important to note that many of the observed truncation products were also found in the 21-day ICR/f rat lens nucleus. A lens at this age has no

Table 1. Top-Down Confirmed Protein Identifications and Their Associated Parameters

Protein ID	Predicted Mass (Da)* (mono/avg)	Residues	Localization (from MALDI Imaging Data)		Solubility (from MALDI Profiling Data)	
			21-day ICR/f	100-day ICR/f	21-day ICR/f	100-day ICR/f
Crystallin, alpha A†	5,053.50 / 5,056.84	1–42	Mostly nuclear	Mostly nuclear	Mostly insoluble	Insoluble
Crystallin, alpha A†	6,409.19 / 6,413.39	1–53	Nuclear	Nuclear	Insoluble	Insoluble
Crystallin, alpha A†	6,565.29 / 6,569.58	1–54	Nuclear	Cortical ring	Insoluble	Insoluble
Crystallin, alpha A†	9,284.76 / 9,290.70	1–78	Nuclear	Nuclear	Insoluble	Insoluble
Crystallin, alpha A†	9,421.80 / 9,427.84	1–79	Nuclear	Mostly nuclear	Insoluble	Insoluble
Crystallin, alpha A†	10,110.11 / 10,116.58	1–85	Mostly nuclear	Nuclear	Insoluble	Insoluble
Crystallin, alpha A†	11,041.61 / 11,048.68	1–93	Nuclear	Nuclear	Insoluble	Insoluble
Crystallin, alpha A†	11,842.04 / 11,849.60	1–100	Nuclear	Mostly nuclear	Insoluble	Insoluble
Crystallin, alpha A†	11,956.08 / 11,963.70	1–101	Nuclear	Mostly nuclear	Sol/insol	Insoluble
Crystallin, alpha A†	17,562.77 / 17,573.90	1–15§	Nuclear ring	Nuclear ring (dispersed)	Mostly insoluble	Mostly insoluble
Crystallin, alpha A†	18,043.96 / 18,055.37	1–156§	Nuclear ring	Nuclear ring (dispersed)	Sol/insol	Mostly insoluble
Crystallin, alpha A†	18,200.06 / 18,211.56	1–157§	Nuclear ring	Nuclear ring (dispersed)	Sol/insol	Sol/insol
Crystallin, alpha A†	18,823.44 / 18,835.32	1–163§	Nuclear ring	Cortical	Sol/insol	Sol/insol
Crystallin, alpha A†	19,393.70 / 19,405.92	1–168§	Nuclear ring	Cortical	soluble	Soluble
Crystallin, alpha A†	19,822.89 / 19,835.35	1–173§	Cortical	Outermost cortical	soluble	Soluble
Alpha-crystallin A chain‡	9,384.59 / 9,390.84	1–79	Nuclear ring	Cortical/Nuclear	Sol/insol	Mostly insoluble
Alpha-crystallin A chain‡	9,837.83 / 9,844.35	1–83	Nuclear ring	Cortical/Nuclear	N/A	Mostly insoluble
Alpha-crystallin A chain‡	22,476.15 / 22,490.49	1–196	Cortical	Outermost cortical	Soluble	Soluble

The identities are correlated with the localization data taken from the MSI experiments as well as the intrinsic solubilities from the MALDI-TOF profiling experiments.

* N-terminal acetylation included (+42.01 Da).

† UniProtKB/TrEMBL A0JN13 (A0JN13_RAT).

‡ UniProtKB/Swiss-Prot P24623 (CRYAA_RAT).

§ Previously identified in ICR/f rat.[17]

opacification,[12] and therefore we conclude that the presence of these species indicates they may not be directly responsible for cataract development in this model. Other events (such as water dysregulation,[12] ionic imbalances,[15]) may initiate cataract formation in the ICR/f lens that leads to the localization changes observed in Figure 4. Therefore, understanding what causes the switch from normal lens protein aging to cataractogenesis is an important question for lens biology, a question that can begin to be answered by studying the truncation products found in other animal models.

The experimental techniques used in this study have added to this understanding, but present limitations. For example, the particular matrix and solvent conditions used in the MSI experiments dictate which signals are measured across the tissue, and only a subset of all expressed proteins are detected in a single MSI analysis. Furthermore, large-molecular-mass aggregates of crystallin proteins, known to correlate with cataract formation, cannot be detected by the current MALDI-TOF instrumentation. Therefore, it is likely that other proteins and protein complexes that were not detected in this study are involved in cataractogenesis. Future work will focus on the identification, tissue distribution, and characterization of solubilities of these and other lens proteins. This work is a beginning in a new and exciting area of study of lens cataracts. With continuing advances in the technology, we will be able to look more rigorously at tissue sections, to understand proteomic changes that occur during cataractogenesis that were previously limited by the specificity and availability of antibodies.

References

1. Bloemendal H, de Jong W, Jaenicke R, Lubsen NH, Slingsby C, Tardieu A. Ageing and vision: structure, stability and function of lens crystallins. *Prog Biophys Mol Biol.* 2004;86:407–485.
2. Bassnett S. Lens organelle degradation. *Exp Eye Res.* 2002;74:1–6.
3. Wistow GJ, Piatigorsky J. Lens crystallins: the evolution and expression of proteins for a highly specialized tissue. *Annu Rev Biochem.* 1988;57:479–504.
4. Augusteyn RC. alpha-crystallin: a review of its structure and function. *Clin Exp Optom.* 2004;87:356–366.
5. Bloemendal H, de Jong WW. Lens proteins and their genes. *Prog Nucleic Acids Res Mol Biol.* 1991;41:259–281.

6. Horwitz J. Alpha-crystallin can function as a molecular chaperone. *Proc Natl Acad Sci U S A.* 1992;89:10449–10453.
7. Horwitz J, Bova MP, Ding LL, Haley DA, Stewart PL. Lens alpha-crystallin: function and structure. *Eye.* 1999;13:403–408.
8. Seeley EH, Caprioli RM. Molecular imaging of proteins in tissues by mass spectrometry. *Proc Natl Acad Sci U S A.* 2008;105:18126–18131.
9. Stoeckli M, Chaurand P, Hallahan DE, Caprioli RM. Imaging mass spectrometry: a new technology for the analysis of protein expression in mammalian tissues. *Nat Med.* 2001;7:493–496.
10. Chaurand P, Caprioli RM. Direct profiling and imaging of peptides and proteins from mammalian cells and tissue sections by mass spectrometry. *Electrophoresis.* 2002;23:3125–3135.
11. Ihara N. A new strain of rat with an inherited cataract. *Experientia.* 1983;39:909–911.
12. Nishida S, Mizuno K, Matubara A, Kurono M. Age-related cataract in the hereditary cataract rat (ICR/1): development and classification. *Ophthalmic Res.* 1992;24:253–259.
13. Yagi K, Komura S, Ihara N, Abe H, Konishi H, Arichi S. Serum lipid peroxide levels in rats with inherited cataracts. *J Appl Biochem.* 1985;7:202–206.
14. Fujii N, Takeuchi N, Tezuka T, et al. Comparison of post-translational modifications of alpha A-crystallin from normal and hereditary cataract rats. *Amino Acids.* 2004;26:147–152.
15. Takeuchi N, Ito H, Namiki K, Kamei A. Effect of calpain on hereditary cataractous rat, ICR/f. *Biol Pharm Bull.* 2001;24:1246–1251.
16. Takeuchi N, Kamei A. Crystallin proteins in lenses of hereditary cataractous rat, ICR/f. *Biol Pharm Bull.* 2000;23:283–290.
17. Takeuchi N, Ouchida A, Kamei A. C-terminal truncation of alpha-crystallin in hereditary cataractous rat lens. *Biol Pharm Bull.* 2004;27:308–314.
18. The UniProt Consortium. The Universal Protein Resource (UniProt). *Nucleic Acids Res.* 2009;37:D169–D174.
19. Bron AJ, Vrensen GF, Koretz J, Maraini G, Harding JJ. The ageing lens. *Ophthalmologica.* 2000;214:86–104.
20. Grey AC, Schey KL. Distribution of bovine and rabbit lens alpha-crystallin products by MALDI imaging mass spectrometry. *Mol Vis.* 2008;14:171–179.
21. Han J, Schey KL. MALDI tissue imaging of ocular lens alpha-crystallin. *Invest Ophthalmol Vis Sci.* 2006;47:2990–2996.
22. Grey AC, Schey KL. Age-related changes in the spatial distribution of human lens alpha-crystallin products by MALDI imaging mass spectrometry. *Invest Ophthalmol Vis Sci.* 2009;50:4319–4329.
23. Truscott RJ. Age-related nuclear cataract-oxidation is the key. *Exp Eye Res.* 2005;80:709–725.
24. Wilmarth PA, Tanner S, Dasari S, et al. Age-related changes in human crystallins determined from comparative analysis of post-translational modifications in young and aged lens: does deamidation contribute to crystallin insolubility? *J Proteome Res.* 2006;5:2554–2566.
25. Zhang X, Dudek EJ, Liu B, et al. Degradation of C-terminal truncated alpha A-crystallins by the ubiquitin-proteasome pathway. *Invest Ophthalmol Vis Sci.* 2007;48:4200–4208.
26. Harding JJ. Free and protein-bound glutathione in normal and cataractous human lenses. *Biochem J.* 1970;117:957–960.
27. Sharma KK, Santhoshkumar P. Lens aging: effects of crystallins. *Biochim Biophys Acta.* 2009;1790:1095–1108.
28. Takemoto L. Release of alpha-A sequence 158-173 correlates with a decrease in the molecular chaperone properties of native alpha-crystallin. *Exp Eye Res.* 1994;59:239–242.
29. van Kleef FS, Nijzink-Maas MJ, Hoenders HJ. Intracellular degradation of alpha-crystallin: fractionation and characterization of degraded alpha A-chains. *Eur J Biochem.* 1974;48:563–570.
30. Aquilina JA, Benesch JL, Ding LL, Yaron O, Horwitz J, Robinson CV. Subunit exchange of polydisperse proteins: mass spectrometry reveals consequences of alphaA-crystallin truncation. *J Biol Chem.* 2005;280:14485–14491.
31. Sweeney MH, Truscott RJ. An impediment to glutathione diffusion in older normal human lenses: a possible precondition for nuclear cataract. *Exp Eye Res.* 1998;67:587–595.
32. Al-Ghoul KJ, Nordgren RK, Kuszak AJ, Freel CD, Costello MJ, Kuszak JR. Structural evidence of human nuclear fiber compaction as a function of ageing and cataractogenesis. *Exp Eye Res.* 2001;72:199–214.
33. Friedrich MG, Truscott RJ. Membrane association of proteins in the aging human lens: profound changes take place in the fifth decade of life. *Invest Ophthalmol Vis Sci.* 2009;50:4786–4793.
34. Greiner JV, Auerbach DB, Leahy CD, Glonek T. Distribution of membrane phospholipids in the crystalline lens. *Invest Ophthalmol Vis Sci.* 1994;35:3739–3746.
35. Korlimbinis A, Berry Y, Thibault D, Schey KL, Truscott RJ. Protein aging: truncation of aquaporin 0 in human lens regions is a continuous age-dependent process. *Exp Eye Res.* 2009;88:966–973.
36. Moffat BA, Landman KA, Truscott RJ, Sweeney MH, Pope JM. Age-related changes in the kinetics of water transport in normal human lenses. *Exp Eye Res.* 1999;69:663–669.
37. Gonen T, Grey AC, Jacobs MD, Donaldson PJ, Kistler J. MP20, the second most abundant lens membrane protein and member of the tetraspanin superfamily, joins the list of ligands of galectin-3. *BMC Cell Biol.* 2001;2:17.
38. Grey AC, Jacobs MD, Gonen T, Kistler J, Donaldson PJ. Insertion of MP20 into lens fibre cell plasma membranes correlates with the formation of an extracellular diffusion barrier. *Exp Eye Res.* 2003;77:567–574.
39. Merck KB, De Haard-Hoekman WA, Oude Essink BB, Bloemendal H, De Jong WW. Expression and aggregation of recombinant alpha A-crystallin and its two domains. *Biochim Biophys Acta.* 1992;1130:267–276.
40. Bova MP, McHaourab HS, Han Y, Fung BK. Subunit exchange of small heat shock proteins: analysis of oligomer formation of alphaA-crystallin and Hsp27 by fluorescence resonance energy transfer and site-directed truncations. *J Biol Chem.* 2000;275:1035–1042.
41. Uga S, Ihara N. Morphological study of a hereditary rat cataract. *Exp Eye Res.* 1990;50:665–670.